Electronic Supplementary Material (ESI) for CrystEngComm.

Understanding the Role of Water in 1,10-Phenanthroline Monohydrate

Doris E. Braun, Anna Schneeberger and Ulrich J. Griesser

Electronic Supplementary Information

Contents of ESI

A. EXPERIMENTAL

1. Room Temperature Solubility Experiments

The room temperature solubility of 1,10-phenanthroline monohydrate was estimated in 24 different solvents. Approx. 10 mg of substance were manually weighted into 1.5 mL vials. 100 mL of solvent were added stepwise under stirring and the solutions were examined visually (Table S1).

Table S1. Estimation of 1,10-Phenanthroline Solubility at 25 °C.

Solvent	Mass (mg)	Dissolved in x mL of solvent
Water	10.14	Insoluble in 1 mL
Methanol	10.26	< 0.1
Ethanol	10.17	< 0.1
2-Propanol	10.24	< 0.1
2-Butanol	10.31	< 0.1
Decanol	10.56	0.3
Acetone	10.26	< 0.1
Acetonitrile	10.02	< 0.1
Chloroform	10.38	0.2
Dichloromethane	10.26	0.2
1,2-Dichloroethane	9.74	0.12
Diethyl ether	10.01	Insoluble in 1 mL
Diisopropyl ether	10.43	Insoluble in 1 mL
Dimethyl formamide	10.16	< 0.1
Dimethyl sulfoxide	10.22	< 0.1
1,4-Dioxane	10.02	0.2
Ethyl acetate	10.13	0.3
Ethyl methyl ketone	10.26	0.2
Methyl isobutyl ketone	10.39	0.4
Nitromethane	10.43	<0.1
Tetrahydrofuran	10.01	0.2
Carbon tetrachloride	10.46	Insoluble in 1 mL
Toluene	10.40	Insoluble in 1 mL
Heptane	10.25	Insoluble in 1 mL

2. Solvent Crystallisation Experiments

2.1. Room Temperature Evaporation Experiments

The saturated solutions prepared in Table S1 were used for evaporation experiments. In case of insolubility in 1 mL the suspensions were heated (50 °C) with stirring, then filtered onto watch glasses. The solvents were allowed to evaporate at RT. Residues were analysed either with IR spectroscopy or powder X-ray diffraction. The results of the evaporative crystallisation screen are summarised in Table S2.

Table S2. Evaporative crystallisation experiments at 25 °C.

Solvent	Microscopic observations	Solid Form[a]
Water		Hy1
Methanol		Hy1
Ethanol		Hy1
2-Propanol		Hy1
2-Butanol		Hy1
Decanol		Hy1
Acetone	Pseudomorphosis	Hy1
Acetonitrile		Hy1
Chloroform		S-Chloroform
Dichloromethane	Pseudomorphosis	Hy1
1,2-Dichloroethane	Pseudomorphosis	Hy1
Diethyl ether		Hy1
Diisopropyl ether		Hy1
Dimethyl formamide		Hy1
Dimethyl sulfoxide		Hy1
1,4-Dioxane		Hy1
Ethyl acetate		Hy1
Ethyl methyl ketone		Hy1
Methyl isobutyl ketone		Hy1
Nitromethane		Hy1
Tetrahydrofuran		Hy1
Carbon tetrachloride		Hy1
Toluene		Hy1
Heptane		Hy1

[a]Hy1 – monohydrate, S – solvate.

2.2. Cooling Crystallisation Experiments

Phenanthroline monohydrate (25 mg) was dissolved close to the boiling point of the solvent. The hot saturated solution was filtered and cooled to room temperature. Within few days solvate crystals were obtained from all four solutions.

Table S3. Cooling Crystallisation experiments.

Solvent	Solid Form
Acetone	S-Acetone
Chloroform	S-Chloroform
Dichloromethane	S-Dichloromethane
1,2-Dichloroethane	S-Dichloroethane

3. Characterisation of *o*-phen Solid Forms

2.3. Anhydrate Polymorphism

The DSC curve in Figure S1 shows the endothermic **AH II** to **AH I°** phase transformation.

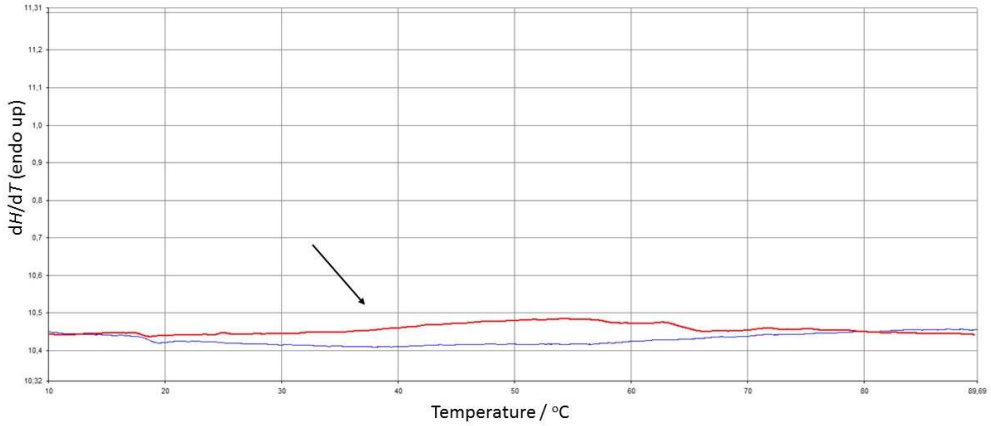

Figure S1. DSC investigations showing the endothermic transformation peak of *o*-phen **AH II** to **AH I°** in the temperature range from 20 to 65 °C (red curve). The arrow indicates the phase transformation. Blue curve corresponds to the blank base line (empty DSC pan).

Low temperature differential scanning calorimetry measurements were performed using a DSC 204 F1 Phoenix (Netzsch-Gerätebau GmbH, Selb, Germany) equipped with a liquid nitrogen cooling device and operated with the Proteus software package version 4.8.5. Approximately 5 milligrams of sample were weighed (Mettler UM3 ultramicrobalance) into sealed Al-pans. Dry nitrogen was used as purge gas (purge: 20 ml min^{-1}) and liquid nitrogen for the cooling process. The measurements were recorded with a heating/cooling rate of 5 °C min^{-1} in the temperature range between –120 to 130 °C. The instrument was calibrated for temperature with Hg (m.p. –38.8°C), benzophenone (48.0 °C), In (156.6 °C), Sn (231.9 °C), Bi (271.4 °C) and Zn (419.6 °C), and the energy calibration was performed with Hg (heat of fusion 11.4 J g^{-1}), In (28.6 J g^{-1}), Sn (60.5 J g^{-1}), Bi (53.1 J g^{-1}) and Zn (60.5 J g^{-1}).

2.4. Monohydrate ↔ Anhydrate Transformation

Infrared spectra were recorded with a heatable diamond ATR (PIKE GaldiATR) crystal on a Bruker Vertex 70 spectrometer (Bruker Analytische Messtechnik GmbH, D). The spectra were recorded in the range of 4000 to 400 cm^{-1} at an instrument resolution of 2 cm^{-1} (64 scans per spectrum).

Variable temperature IR spectroscopy was applied to monitor the change of *o*-phen **Hy1** in the temperature range starting from 25 °C to 130 °C. In agreement with the HSM, TGA and DSC experiments a phase transformation to **AH I°** is observed at temperatures starting from 80 °C (Figure S2). The dehydration is indicated by the loss of intensity of the ν(OH) and δ(OH) vibrations (3363 cm^{-1} and 1640 cm^{-1}).

In a second experiment the hydration of **AH I°** was monitored time resolved (Figure S3) at 25 °C and 25% RH. Transformation to **Hy1** starts immediately, and within 10 minutes a complete transformation is observed.

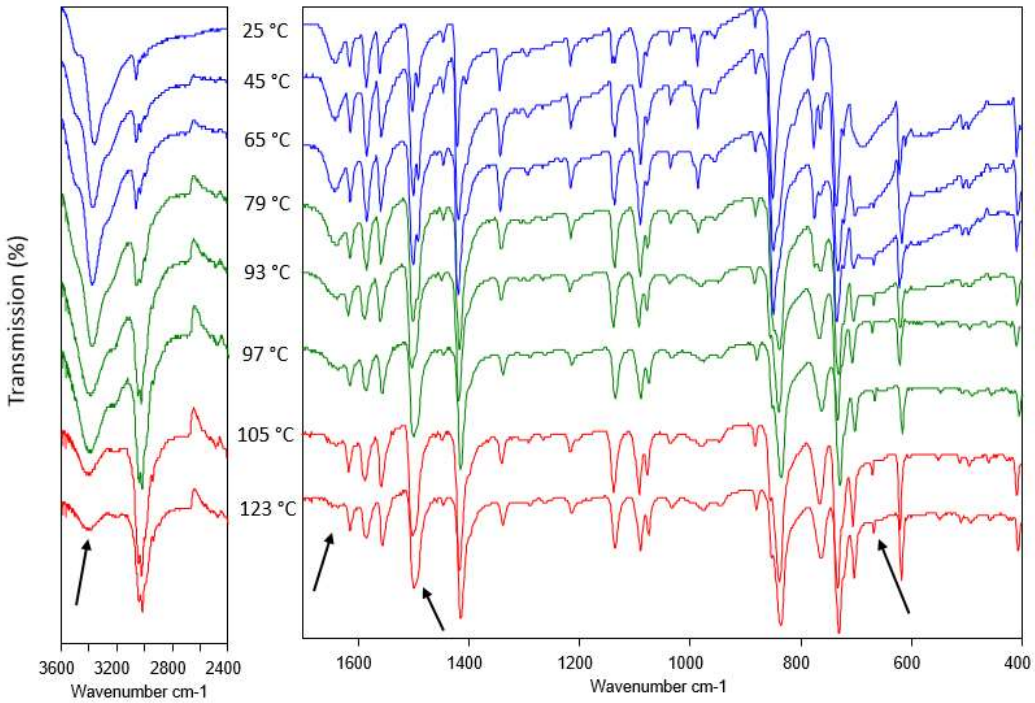

Figure S2. *O*-Phen **Hy1** to **AH I°** transformation monitored with variable temperature IR spectroscopy. Blue spectra correspond to **Hy1**, green to **Hy1** > **AH I°** and red to **AH I°** > **Hy1**. Arrows denote characteristic bands of **Hy1**. Note that the dehydration was not completed in the course of the experiment.

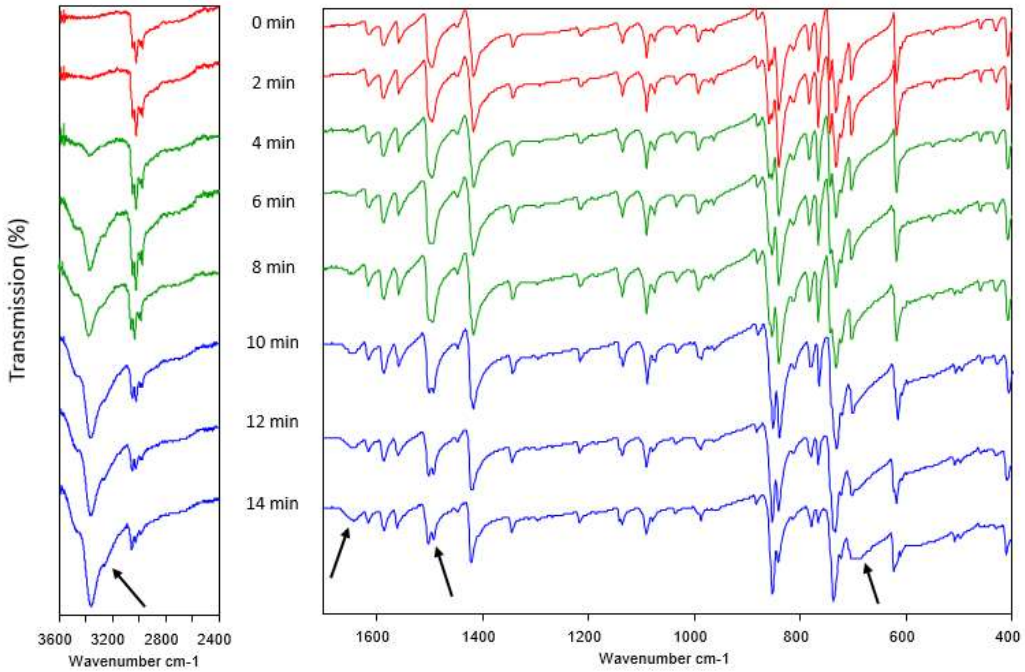

Figure S3. *O*-Phen **AH I°** to **Hy1** transformation monitored with IR spectroscopy. Red spectra correspond to **AH I°**, green to a mixture of the two forms and blue to **Hy1**. Arrows denote characteristic bands of **Hy1**.

2.5. Chloroform Solvate

Thermal Analysis

By embedding the chloroform solvate crystals in silicon oil it is possible the monitor the desovlation process upon heating. The formation of bubbles at 70 °C indicates the loss of solvent (Figure S4).

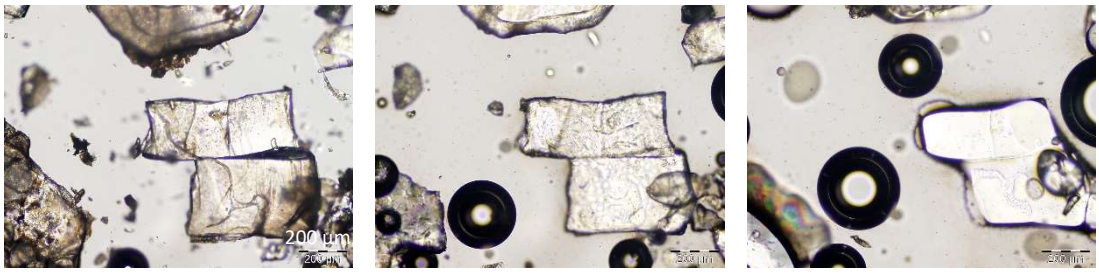

A) 50 °C B) 80 °C C) 110 °C

Figure S4. Hot-stage microscopic investigations showing the desolvation of the *o*-phen chloroform monosolvate in the temperature range from 50 °C to 110 °C. The crystals were embedded in silion oil.

The TGA experiments of the chloroform solvate confirmed the presence of a monosolvate (Figure S5). The experimentally derived mass loss is 40.8 ± 0.6 % and agrees well with the theoretical value of a monosolvate of 39.9%.

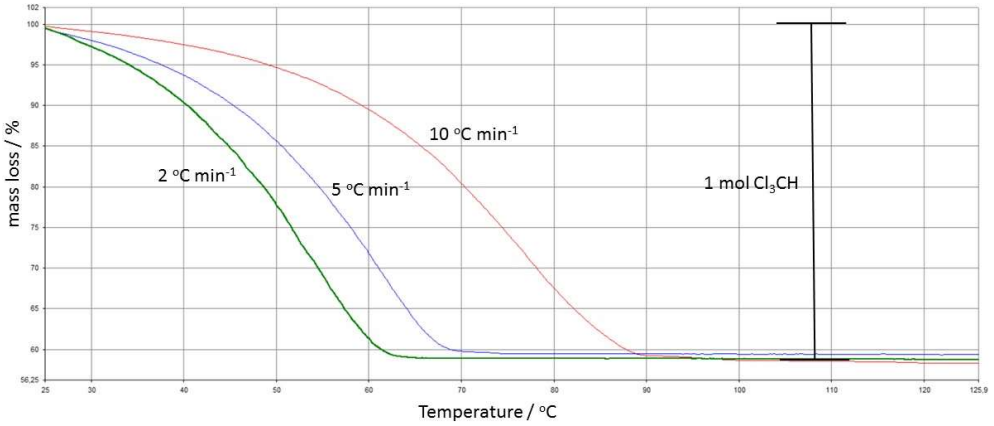

Figure S5. Thermogravimetric analysis of *o*-phen chloroform monosolvate, recorded in the temperature range starting from 25 °C to 130 °C using heating rates of 2, 5 and 10 °C min^{-1}.

Infrared Spectroscopy

The desolvation of the chloroform monosolvate was monitored with IR spectroscopy (ATR). Figure S6 shows the IR spectra recorded upon heating the solvate sample. In the temperature range from 25 °C to 90 °C the sovlate is stable. Starting from 95 °C, desolvation is observed, indicated by the decrease in intensity of the ν(C-H) vibration (2934 cm^{-1}) of the chloroform molecule. It has to be noted that desolvation was not completed at the end of the experiment.

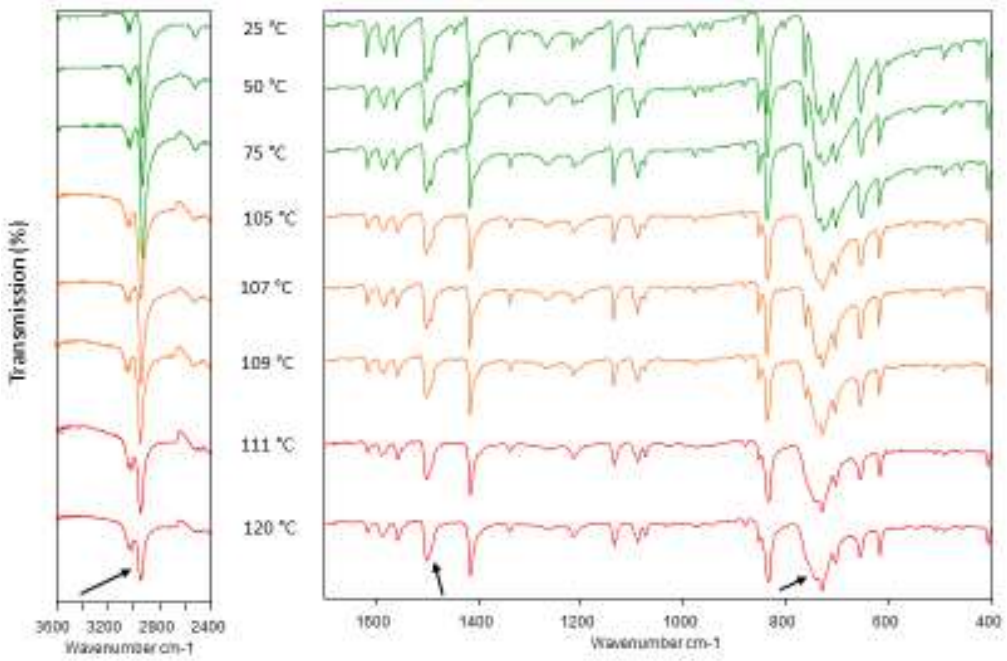

Figure S6. Heating IR spectroscopy experiments (ATR), showing the transformation of the chloroform solvate to **AH I°**. Temperature values correspond to the recording temperature. Arrows mark differences seen in the IR spectra.

In a second experiment (Figure S7) the transformation of the chloroform solvate to the monohydrate was monitored with IR spectroscopy (25% RH, RT). Within few minutes, hydration of the sample is evident from the appearance of the ν(OH) vibrations at 3363 cm^{-1} and the δ(OH) vibrations at 1640 cm^{-1}.

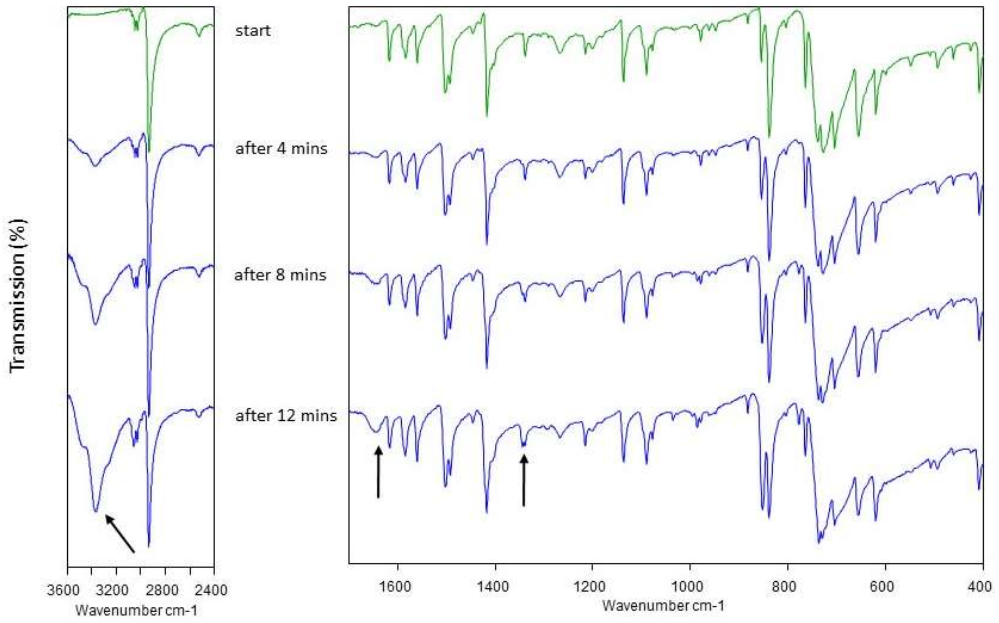

Figure S7. Time-resolved IR spectroscopy experiments (ATR), showing the transformation of the chloroform solvate to **Hy1**. Arrows mark differences seen in the IR spectra.

2.6. Acetone Solvate

The acetone solvate was prepared by cooling a hot saturated chloroform solution of *o*-phen slowly to RT. Crystallisation of the solvate occurred within two days. The acetone solvate crystals are very unstable. Removal of the crystals from the mother liquor results in a transformation to **Hy1** within few seconds at ambient conditions (Figure S8).

A) Solvate crystals in mother liquor

B) after 8 seconds

C) after 10 second

Figure S8. Solvate to **Hy1** transformation of *o*-phen acetone solvate crystals after removing from the mother liquor. Transformation is highlighted with red ellipsoids for clarity.

2.7. Dichloromethane Solvate

Cooling a hot saturated *o*-phen dichloromethane solution to RT leads to the formation of the dichloromethane solvate. The solvate crystals are very unstable at ambient conditions. Removal of the crystals from the mother liquor results in a transformation to **Hy1** within few seconds at ambient conditions (Figure S9).

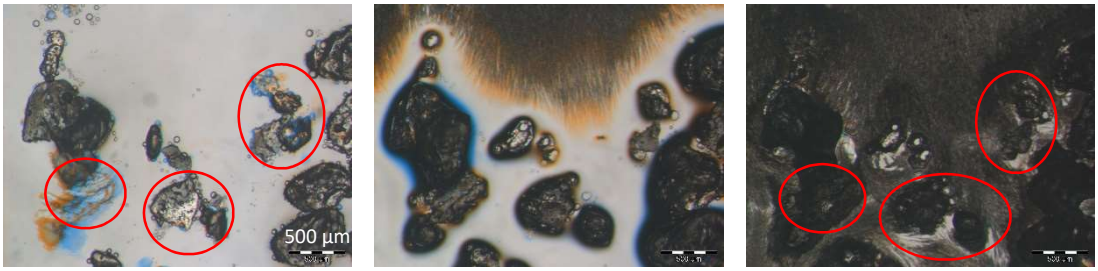

A) Solvate crystals in mother liquor

B) after 6 seconds

C) after 10 seconds

Figure S9. Solvate to **Hy1** transformation of *o*-phen dichloromethane solvate crystals after removing from the mother liquor. Transformation is highlighted with red ellipsoids for clarity.

2.8. 1,2-Dichloroethane Solvate

1,2-Dichloroethane solvate crystals were prepared as described for the dichloromethane sovlate. The solvate crystals are very unstable at ambient conditions. Removal from its mother liquor results in a transformation to **Hy1** within few seconds (ambient conditions).

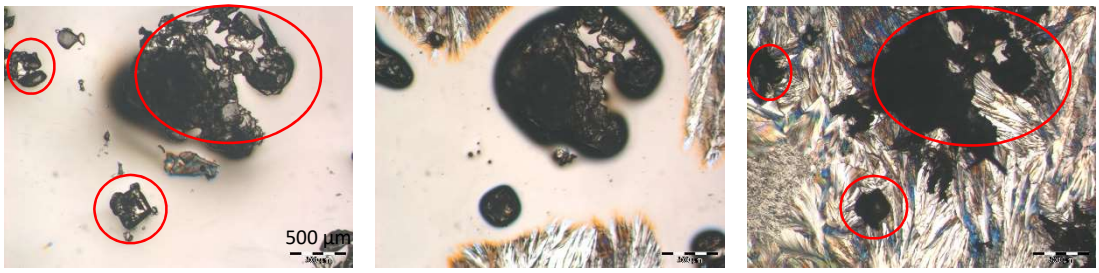

A) Solvate crystals in mother liquor

B) after 6 seconds

C) after 10 seconds

Figure S10. Solvate to **Hy1** transformation of *o*-phen dichloroethane solvate crystals after removing from the mother liquor. Transformation is highlighted with red ellipsoids for clarity.

B. MODELLING

4. CASTEP Lattice Energy Minimisations

The DFT-D calculations were carried out with the CASTEP plane wave code (v. 6.1)[1] using the Perdew-Burke-Ernzerhof (PBE) generalised gradient approximation (GGA) exchange-correlation density functional[2] and ultrasoft pseudopotentials,[3] with the addition of a semi-empirical dispersion correction, either the Tkatchenko and Scheffler (TS) model,[4] or Grimme06 (D2).[5] In a first step, the structures were geometry optimised using the TS dispersion correction. Brillouin zone integrations were performed on a symmetrised Monkhorst–Pack *k*-point grid with the number of *k*-points chosen to provide a maximum spacing of 0.07 $Å^{-1}$ and a basis set cut-off of 780 eV. The self-consistent field convergence on total energy was set to $1x10^{-5}$ eV. Energy minimisations were performed using the Broyden–Fletcher–Goldfarb–Shanno optimisation scheme within the space group constraints. The optimisations were considered complete when energies were converged to better than $2x10^{-5}$ eV per atom, atomic displacements converged to $1x10^{-3}$ Å, maximum forces to $5x10^{-2}$ eV $Å^{-1}$, and maximum stresses were converged to $1x10^{-1}$ GPa. The energies for the structures were recalculated, without optimisation, with the number of *k*-points chosen to provide a maximum spacing of 0.07 $Å^{-1}$ and a basis set cut-off of 780 eV, using the D2 dispersion correction. Isolated molecule minimisations to compute the isolated *o*-phen and H_2O were performed by placing a single molecule in a fixed cubic 35x35x35 $Å^3$ unit cell, then optimised with the same settings as used for the crystal calculations.

5. Computationally Generated Low-Energy Monohydrate Structures

All calculated structures are available in .res format from the authors on request. The lowest energy PBE-TS structures are given in Table S4.

Table S4. Known and computationally generated low energy *o*-phen monohydrate (PBE-TS optimised and PBE-D2 single point calculations) structures. The experimental structure is highlighted in grey.

Str.[a]	Space group	Cell parameters						E_{latt}/ kJ mol^{-1}	PI[b]/ %	H-bonding[c]	water[d]
		a/Å	*b*/Å	*c*/Å	*α*/°	*β*/°	*γ*/°				
01_MH	$P3_2$ ($P3_1$)	17.338	17.338	8.383	90	90	120	–186.11	73.3	3x DDA	chain
02_3064	$P2_12_12_1$	4.623	14.320	14.348	90	90	90	–184.15	74.9	DDA	chain
03_3152	$P3_2$ ($P3_1$)	10.466	10.466	7.777	90	90	120	–182.23	72.4	DDA	chain
04_2389	$P2_12_12_1$	4.566	13.729	15.095	90	90	90	–182.23	75.4	DDA	chain
05_1945	$Pna2_1$	4.595	14.642	14.544	90	90	90	–181.99	72.5	DDA	chain
06_3267	$Pna2_1$	4.584	14.413	14.772	90	90	90	–181.79	72.9	DDA	chain
07_7249	$P4_2/n$	22.387	22.387	3.770	90	90	90	–180.46	75.3	DD	bridge
08_2877	$P3_2$ ($P3_1$)	10.108	10.108	8.374	90	90	120	–180.29	72.0	DDA	chain
09_6660	$P2_12_12_1$	4.495	13.777	15.181	90	90	90	–179.64	75.8	DDA	chain
10_1115	$P2_1/n$	3.753	16.029	15.869	90	95.39	90	–179.15	75.0	DD	bridge
11_842	$P2_12_12_1$	4.608	13.862	14.886	90	90	90	–178.93	74.8	DDA	chain
12_1496	$I4_1/a$	14.832	14.832	17.436	90	90	90	–178.80	74.2	DDA	H-tetr.
13_1228	$P2_12_12_1$	5.706	12.226	13.876	90	90	90	–178.52	73.6	DD	bridge
14_8637	$P\bar{1}$	7.541	7.652	9.541	108.81	104.25	104.47	–177.68	75.6	DD	bridge
15_6941	$P\bar{1}$	7.690	7.735	9.264	105.85	106.57	103.84	–177.15	74.6	DD	bridge
16_172	$P1$	3.723	8.040	8.333	69.81	88.99	83.81	–176.42	76.8	DD	bridge
17_1154	$Pca2_1$	16.078	3.722	15.770	90	90	90	–176.32	75.6	DD	bridge
18_9313	$P\bar{1}$	7.970	8.598	8.910	104.60	116.02	104.53	–176.18	74.0	DD	bridge
19_461	$P2_1/c$	9.347	12.184	9.405	90	118.37	90	–175.99	75.9	DD	bridge
20_165	$Pna2_1$	8.122	3.660	15.984	90	100.47	90	–175.80	76.4	DD	bridge
21_84	$I4_1/a$	13.672	13.672	20.293	90	90	90	–175.70	75.5	DD	bridge
22_234	$P2_1/c$	7.325	16.094	8.775	90	112.28	90	–175.27	74.5	DD	bridge
23_289	$I2/c$	16.128	7.244	18.116	90	113.03	90	–175.08	73.2	DD	bridge
24_5982	$Pbca$	11.696	11.913	14.253	90	90	90	–175.07	71.4	DD	bridge
25_285	$P2_1/c$	7.761	17.424	7.352	90	104.16	90	–175.02	73.9	DD	bridge
26_4082	$P2_1/c$	6.191	10.917	14.343	90	94.77	90	–174.23	73.9	DD	bridge
27_7303	$P2_1/n$	6.289	11.757	13.538	90	93.63	90	–174.10	73.1	DD	bridge
28_3611	Pn	9.741	3.665	13.288	90	92.43	90	–173.87	75.4	DD	bridge
29_557	$P\bar{1}$	7.847	8.214	8.968	106.95	113.99	99.30	–173.83	74.7	DD	bridge
30_40	$P\bar{1}$	7.436	8.533	8.854	106.11	97.88	109.46	–173.48	72.4	DD	bridge
31_1249	$C2/c$	18.123	7.415	15.421	90	110.53	90	–173.43	73.8	DD	bridge
32_4586	$P2_1/c$	8.918	11.232	10.240	90	106.51	90	–172.82	72.7	DD	ring
33_9300	$Pbca$	15.512	7.160	17.612	90	90	90	–172.66	72.8	DD	bridge
34_5978	$P2_1/n$	9.549	7.064	14.410	90	91.14	90	–172.51	73.3	DD	bridge
35_254	$P2_1/n$	9.407	10.044	10.108	90	91.15	90	–172.50	74.8	DD	bridge
36_685	$P2_1/c$	4.638	15.686	13.530	90	98.37	90	–171.55	73.2	DD	bridge
37_1167	$P2_1/n$	7.144	9.576	14.545	90	101.22	90	–171.52	73.2	DD	bridge
38_710	$P2_1/n$	6.233	10.890	14.613	90	102.28	90	–171.28	73.7	DD	bridge
39_26	$P\bar{1}$	7.774	7.917	9.411	106.24	104.39	110.76	–171.02	74.7	DD	bridge

Str.	Space group	Cell parameters						E_{latt}/ kJ mol^{-1}	PI/ %	H-bonding	water
		a/Å	*b*/Å	*c*/Å	*α*/°	*β*/°	*γ*/°				
40_4419	*Pbca*	15.091	8.593	15.241	90	90	90	–170.90	72.3	DD	bridge
41_9922	*C*2/*c*	15.376	10.485	13.145	90	108.27	90	–170.82	71.1	DD	bridge
42_9251	$P2_12_12$	11.071	14.883	6.074	90	90	90	–170.65	71.1	DD	bridge
43_999	*C*2/*c*	13.574	10.474	14.021	90	97.22	90	–170.62	72.1	DD	bridge
44_310	$P2_1/n$	9.305	10.207	10.338	90	93.01	90	–170.28	72.9	DD	bridge
45_73	$P2_1/n$	9.062	10.045	10.928	90	93.49	90	–169.86	71.9	DD	bridge
46_7607	$P2_1/c$	8.859	15.568	7.153	90	94.81	90	–169.57	72.6	DD	bridge
47_1165	$P2_1/n$	6.135	11.343	14.407	90	96.19	90	–169.22	71.6	DD	bridge
48_1014	$P2_1/n$	4.829	14.123	14.318	90	91.04	90	–169.15	73.0	DD	bridge
49_2351	$P2_1/c$	5.525	12.528	14.575	90	98.52	90	–169.04	71.6	DD	bridge
50_3372	$P2_1/n$	9.533	7.255	14.871	90	106.90	90	–168.75	72.6	DD	ring
51_5963	$P2_1/n$	11.197	6.150	14.552	90	97.73	90	–168.36	72.0	DD	bridge
52_5064	$P2_1/n$	10.501	6.758	14.039	90	95.03	90	–168.13	71.9	DD	bridge
53_103	*C*2/*c*	13.883	10.398	13.835	90	97.74	90	–167.21	72.2	DD	bridge

[a]Structure ID: rank PBE-D2_rank CrystalPredictor. [b]Packing Index calculated using PLATON.[6] [c]water environment type (D – H-bonding donor, A – H-bonding acceptor)[7]. [d]Figure 8b.

6. Representation of the Experimental Structures

The computational models were successful in reproducing the experimental structures (Table S5). The structures were compared using the Molecular Similarity Module in Mercury to determine the root mean square deviation of the non-hydrogen atoms in a cluster of *n* molecules ($rmsd_n$).[8]

Table S5. Quality of representation of the experimental PBE-TS anhydrate and monohydrate structures.

Solid Form	Lattice parameters (cell vectors/Å, angles/°)						Density / g cm^{-3}	$rmsd_n$ (Å)
	a	*b*	*c*	*α*	*β*	*γ*		
Anhydrate								
OPENAN, *C*2, 298 K	19.914(3)	7.405(1)	9.451(1)	90	99.60 (1)	90	1.307	0.124 (*n*=15)
PBE-TS, 0 K	19.7619	7.1636	9.3906	90	99.466	90	1.369	–
Monohydrate								
ZZZAMS03, $P3_1$, 298 K	17.833(3)	17.833(3)	8.543(1)	90	90	120	1.259	–
ZZZAMS04, $P3_1$, 298 K	17.792(2)	17.792(2)	8.5221(5)	90	90	120	1.268	0.207 (*n*=30)
ZZZAMS05, $P3_1$, 173 K	17.6921(6)	17.6921(6)	8.4921(6)	90	90	120	1.286	0.155 (*n*=30)
ZZZAMS06, $P3_2$, 100 K	17.5216(9)	17.5216(9)	8.4337(4)	90	90	120	1.321	0.084 (*n*=30)
ZZZAMS07, $P3_2$, 100 K	17.5216(9)	17.5216(9)	8.4337(4)	90	90	120	1.321	0.084 (*n*=30)
PBE-TS, 0K	17.3377	17.3377	8.3825	90	90	120	1.358	–

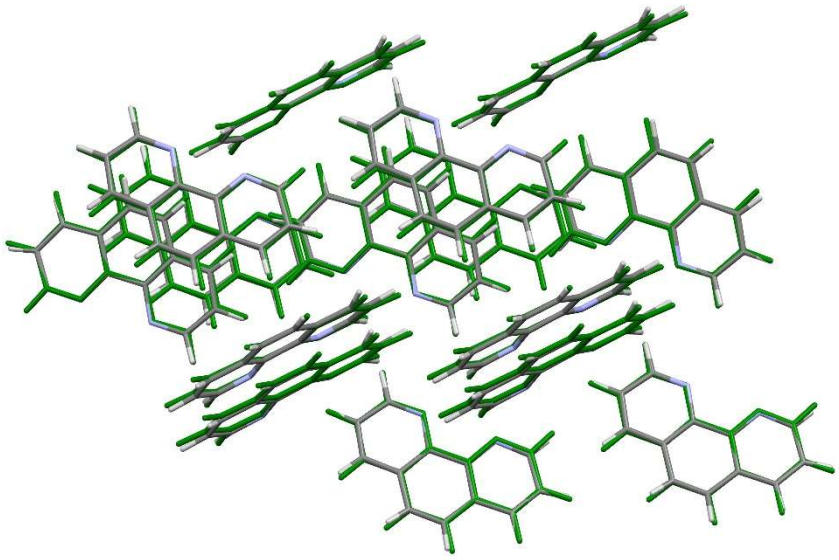

Figure S11. Overlay of the 15 molecule cluster of the observed structure of *o*-phen **AH I°** (coloured by element) and calculated PBE-TS structure (green), $rmsd_{15}$=0.12 Å.

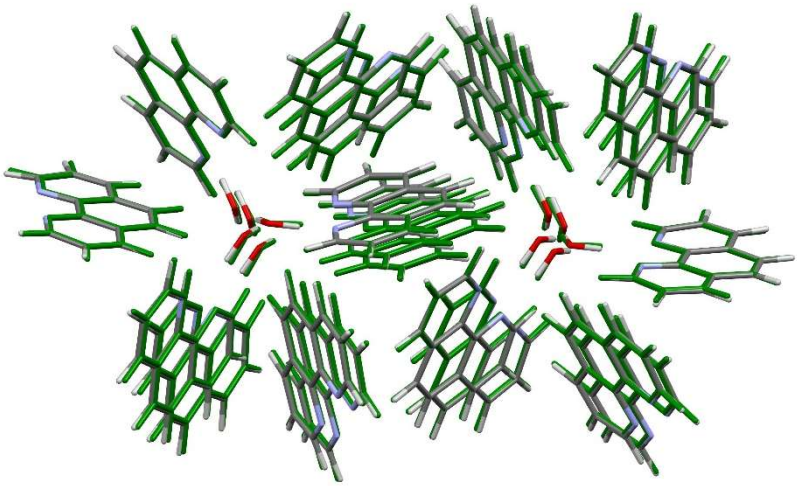

Figure S12. Overlay of the 30 molecule cluster of the observed structure of *o*-phen **Hy1** (ZZZAMS07, coloured by element) and calculated PBE-TS structure (green), $rmsd_{30}$=0.08 Å.

7. PIXEL Intermolecular Energy Calculations

PIXEL energies are intermolecular energies (i.e. U_{inter}) derived by integration over the isolated molecule charge densities placed in the crystal structures. The electrostatic contribution E_C is rigorously derived by this procedure and various approximations are used to estimate the polarisation (induction) E_P, dispersion E_D, and repulsion E_R contribution to the intermolecular lattice energy. The calculations also provide an approximate breakdown into contributions from different pairs of molecules in the coordination shell.

It has to be noted that the non-additivity of the molecule···molecule polarisation energies could not be taken into account for calculating the pair-wise energies given in Table 1. This error was estimated by considering the lattice energies obtained by summing the molecule-molecule pairwise energies. These energies differ from the PIXEL lattice energies when the polarisation is calculated from the net field (i.e. accounting for non-additivity of the electrostatic field around a molecule) by max. 4.7%. Thus, the neglect of non-additivity does not qualitatively affect the results discussed in the m/s.

Table S6. PIXEL intermolecular energy calculations on **AH I°** and selected low energy monohydrate structures. Only the most relevant intermolecular interactions for pairs of molecules are listed.

Structure	Interaction[a]	E_C[b]	E_P[c]	E_D[d]	E_R[e]	U_{inter}[f]
		kJ mol^{-1}				
Anhydrate	A···B (6.913)	-15.7	-7.2	-19.4	13.6	-28.7
(Z'=2)	B···B (7.164)	-11.4	-7.7	-19.1	14.9	-23.4
*C*2	A···B (6.146)	-6.2	-4.7	-26.3	18.7	-18.5
	A···B (7.539)	-10.1	-4.2	-15.9	14.1	-16.1
	A···B (6.803)	-11.7	-8.1	-20.2	25.1	-15.0
Hydrate	A···W (4.231)	-56.3	-25.6	-16.2	59.1	-39.1
02_3064	A···A (4.623)	-9.1	-6.3	-54.9	45.4	-25.0
$P2_12_12_1$	W···W (2.750)	-54.9	-21.5	-8.3	61.1	-23.6
	A···W (5.848)	-11.0	-2.0	-4.7	4.2	-13.5
	A···W (5.687)	-8.0	-2.7	-5.5	5.6	-10.7
	A···A (7.643)	-4.6	-3.1	-16.2	13.6	-10.3
Hydrate	A···W (4.228)	-47.4	-22.1	-15.0	51.2	-33.2
07_7249	A···W (4.111)	-43.3	-20.1	-15.3	48.6	-30.1
$P4_2/n$	A···A (3.770)	0.1	-6.2	-59.8	41.7	-24.2
	A···A (8.375)	-8.0	-2.5	-11.1	8.3	-13.4
	A···W (5.359)	-12.7	-4.9	-8.6	13.5	-12.7
	A···A (8.505)	-6.2	-2.6	-10.7	8.0	-11.5
	A···W (5.915)	-10.9	-3.9	-6.2	11.5	-9.6
Hydrate	A···W (4.161)	-63.9	-28.8	-17.2	69.2	-40.6
08_2877	A···A (5.788)	-16.4	-7.7	-29.5	29.0	-24.5
$P3_2$	A···A (5.828)	-16.8	-7.6	-29.2	29.2	-24.4
	W···W (2.942)	-32.6	-10.6	-6.2	26.4	-22.8
	A···W (5.848)	-12.0	-2.6	-5.5	6.9	-13.3
	A···A (7.541)	-4.6	-2.0	-15.5	9.4	-12.7
	A···A (7.573)	-4.1	-1.5	-13.2	6.5	-12.4

[a]PIXEL energies are for a pair of molecules. The pairs of molecules are defined by the distance between their centers of mass in Å. A and B – symmetry independent *o*-phen molecules, W – water; [b]electrostatic (Coulombic) energy; [c]polarisation energy; [d]dispersion energy; [e]repulsion energy; [f]total intermolecular energy: $U_{inter} = E_C + E_P + E_D + E_R$. The non-additivity of E_P is not included.

Figure S13 to Figure S15 illustrate the strongest intermolecular interactions found in the computationally generated monohydrate structures 02_3064, 07_7249 and 08_2877.

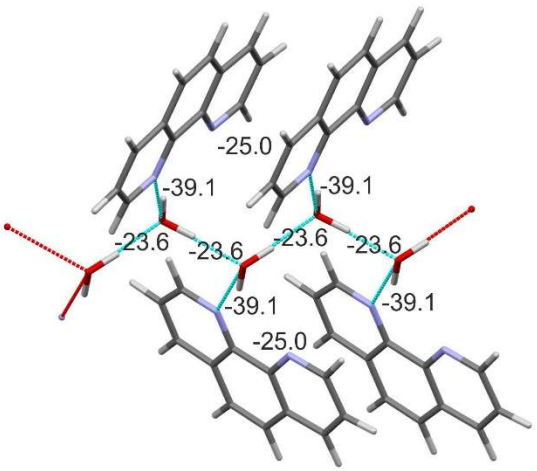

Figure S13. Computationally generated monohydrate structure 02_3064, with water molecules forming a water chain. Numbers in kJ mol^{-1} correspond to the pair-wise intermolecular energies (derived using PIXEL).

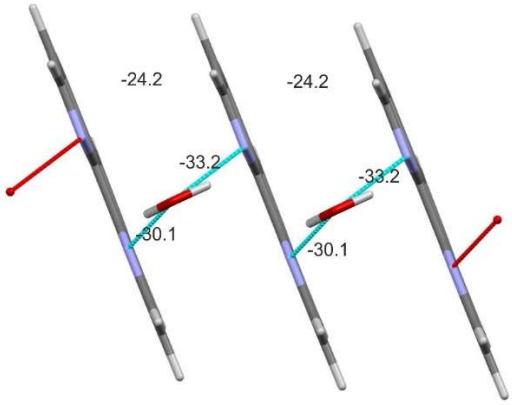

Figure S14. Computationally generated monohydrate structure 07_7249, with water molecules forming a water chain. Numbers in kJ mol^{-1} correspond to the pair-wise intermolecular energies (derived using PIXEL).

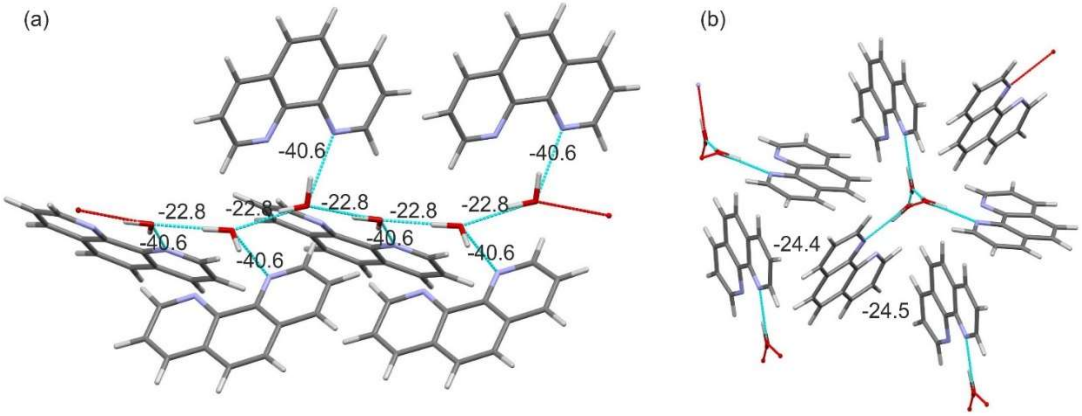

Figure S15. Computationally generated monohydrate structure 08_2877, with water molecules forming a water chain. Numbers in kJ mol^{-1} correspond to the pair-wise intermolecular energies (derived using PIXEL).

8. Computationally Generated Monohydrate Structures

The .res files for the computationally generated Z'=1 monohydrate structures are given below.

8.1. Structure 3

```
TITL 3_3152
CELL 0.71073 10.4656 10.4656 7.7766 90 90 120
ZERR 3 0.0000 0.0000 0.0000 0 0 0
LATT -1
SYMM -y,x-y,2/3+z
SYMM -x+y,-x,1/3+z
SFAC C H N O
UNIT 36 30 6 3
FVAR 1.00
C1      1  0.335730  0.198790  0.504090  1.000000 0.05000
C2      1  0.105530  0.188850  0.450740  1.000000 0.05000
C3      1  0.212460  0.157520  0.397870  1.000000 0.05000
C4      1  0.120480  0.259000  0.610010  1.000000 0.05000
C5      1  0.016590  0.299660  0.668910  1.000000 0.05000
C6      1  0.035940  0.369780  0.822600  1.000000 0.05000
C7      1  0.157180  0.398360  0.931880  1.000000 0.05000
C8      1  0.177590  0.464860  1.094820  1.000000 0.05000
C9      1  0.295390  0.487380  1.195680  1.000000 0.05000
C10     1  0.391270  0.440350  1.133970  1.000000 0.05000
C11     1  0.261190  0.356760  0.878880  1.000000 0.05000
C12     1  0.246000  0.291000  0.711440  1.000000 0.05000
H1      2  0.425370  0.180510  0.464460  1.000000 0.06000
H2      2  0.011190  0.163350  0.369530  1.000000 0.06000
H3      2  0.204590  0.105370  0.274340  1.000000 0.06000
H4      2 -0.078710  0.274710  0.589020  1.000000 0.06000
H5      2 -0.043030  0.402450  0.865240  1.000000 0.06000
H6      2  0.098430  0.496100  1.139500  1.000000 0.06000
H7      2  0.313380  0.537960  1.322300  1.000000 0.06000
H8      2  0.483560  0.451900  1.211040  1.000000 0.06000
H9      2  0.804520  0.482010  0.258920  1.000000 0.06000
H10     2  0.690700  0.356570  0.380700  1.000000 0.06000
N1      3  0.352800  0.262890  0.657110  1.000000 0.05000
N2      3  0.375630  0.377440  0.980480  1.000000 0.05000
O1      4  0.699990  0.400240  0.264340  1.000000 0.05000
END
```

8.2. Structure 8

```
TITL 08_2877
CELL 0.71073 10.1077 10.1077 8.3738 90 90 120
ZERR 3 0.0000 0.0000 0.0000 0 0 0
LATT -1
SYMM -y,x-y,2/3+z
SYMM -x+y,-x,1/3+z
SFAC C H N O
UNIT 36 30 6 3
FVAR 1.00
C1      1 -0.110540  0.263140 -0.171710  1.000000 0.05000
C2      1 -0.150600  0.361260 -0.249650  1.000000 0.05000
C3      1 -0.120100  0.495140 -0.174800  1.000000 0.05000
C4      1 -0.056930  0.526970 -0.020160  1.000000 0.05000
C5      1 -0.022900  0.663740  0.063150  1.000000 0.05000
C6      1  0.039210  0.691620  0.212250  1.000000 0.05000
C7      1  0.065130  0.581360  0.291370  1.000000 0.05000
C8      1  0.125590  0.604460  0.446850  1.000000 0.05000
C9      1  0.148300  0.494480  0.517990  1.000000 0.05000
C10     1  0.104740  0.358300  0.434800  1.000000 0.05000
C11     1  0.029690  0.442580  0.213620  1.000000 0.05000
C12     1 -0.026650  0.417660  0.051700  1.000000 0.05000
H1      2 -0.126460  0.159080 -0.228840  1.000000 0.06000
H2      2 -0.143200  0.577830 -0.232930  1.000000 0.06000
H3      2 -0.201270  0.332910 -0.368420  1.000000 0.06000
H4      2 -0.045680  0.746230  0.003830  1.000000 0.06000
H5      2  0.071610  0.799110  0.272770  1.000000 0.06000
H6      2  0.152070  0.709090  0.509490  1.000000 0.06000
H7      2  0.195820  0.510480  0.637750  1.000000 0.06000
H8      2  0.114650  0.265300  0.488950  1.000000 0.06000
H9      2 -0.009320  0.027980  0.056880  1.000000 0.06000
H10     2  0.010880  0.151860  0.185330  1.000000 0.06000
N1      3 -0.050010  0.289740 -0.025680  1.000000 0.05000
N2      3  0.047400  0.332480  0.286980  1.000000 0.05000
O1      4  0.000160  0.048620  0.172930  1.000000 0.05000
END
```

References

1. Clark, S. J.; Segall, M. D.; Pickard, C. J.; Hasnip, P. J.; Probert, M. J.; Refson, K.; Payne, M. C., First principles methods using CASTEP. *Zeitschrift fur Kristallographie* **2005,** *220* (5-6), 567-570.
2. Perdew, J. P.; Burke, K.; Ernzerhof, M., Generalized gradient approximation made simple. *Physical Review Letters* **1996,** *77* (18), 3865-3868.
3. Vanderbilt, D., Soft Self-Consistent Pseudopotentials in a Generalized Eigenvalue Formalism. *Physical Review B* **1990,** *41* (11), 7892-7895.
4. Tkatchenko, A.; Scheffler, M., Accurate Molecular Van Der Waals Interactions from Ground-State Electron Density and Free-Atom Reference Data. *Phys. Rev. Lett* **2009,** *102* (7), 073005/1-073005/4.
5. Grimme, S., Semiempirical GGA-type density functional constructed with a long-range dispersion correction. *J. Comput. Chem* **2006,** *27* (15), 1787-1799.
6. Spek, A. L. *PLATON, A Multipurpose Crystallographic Tool*, Utrecht University: Utrecht, The Netherlands, 2003.
7. Infantes, L.; Fabian, L.; Motherwell, W. D. S., Organic crystal hydrates: what are the important factors for formation. *CrystEngComm* **2007,** *9* (1), 65-71.
8. Chisholm, J. A.; Motherwell, S., COMPACK: a program for identifying crystal structure similarity using distances. *Journal of Applied Crystallography* **2005,** *38*, 228-231.